

# Relativistic Heavy-Ion Physics: Experimental Overview

Itzhak Tserruya <sup>1</sup>

Department of Particle Physics, Weizmann Institute,  
Rehovot 76100, Israel

## Abstract

The field of relativistic heavy-ion physics is reviewed with emphasis on new results and highlights from the first run of the Relativistic Heavy-Ion Collider at BNL and the 15 year research programme at the SPS at CERN and the AGS at BNL.

Invited Talk at the Fourth International Conference on Physics and Astrophysics of Quark Gluon Plasma, (ICPAQGP-2001) Jaipur, India, November 26-30, 2001.

---

<sup>1</sup>e-mail: Itzhak.Tserruya@weizmann.ac.il.

Work supported by the Israeli Science Foundation and the Nella and Leon Benozio Center of High Energy Physics Research.

# 1 INTRODUCTION

The field of relativistic heavy-ion collisions is at a unique time in its development. The Relativistic Heavy-Ion Collider (RHIC) at BNL started regular operation in the summer of year 2000. In a very short, but extremely successful, run with an integrated luminosity of only a few  $\mu b^{-1}$ , the four RHIC experiments delivered an impressive amount of results offering a first glimpse at the physics of Au-Au collisions at the energy of  $\sqrt{s_{NN}} = 130 \text{ GeV}$ , almost one order of magnitude larger than the highest energy of  $\sqrt{s_{NN}} = 17.2 \text{ GeV}$  available at CERN. Some of these results are new and exciting, some are puzzling and some follow the pattern already established at lower energies. A lot more is expected to come from the second run at the design energy of  $\sqrt{s_{NN}} = 200 \text{ GeV}$ , completed by the time of this conference with almost two orders of magnitude larger integrated luminosity. In addition to that, the 15 year programme at CERN SPS and BNL AGS has produced a wealth of very interesting and intriguing results and more is still to be expected from the SPS in the next few years. This combination results in very exciting opportunities for the study of matter under extreme conditions and in particular for the quest of the phase transition associated with quark-gluon plasma formation and chiral symmetry restoration.

About a dozen of different experiments at the AGS and SPS and four experiments at RHIC are or have been involved in this endeavour covering a very broad range of observables. In the limited space of this paper it is not possible to do justice to the vast amount of available results [1]. A selection is therefore unavoidable and this review is restricted to selected topics on recent results and highlights of the field on: (i) global observables where systematic comparisons are made from AGS up to RHIC energies (Section 2), (ii) hadron spectra and yields (Section 3), (iii) excess emission of low-mass lepton pairs (Section 4) and  $J/\psi$  suppression (Section 5) which are among the most notable results hinting at new physics from the SPS programme (results on these two topics are not yet available at RHIC as they require a much higher luminosity than achieved in the first year), and (iv) suppression of large  $p_T$  hadrons (Section 6) which is one of the highlights of the first RHIC run pointing to new phenomena opening up at RHIC energies.

## 2 GLOBAL OBSERVABLES

### 2.1 $N_{ch}$ and $E_T$ distributions

Global observables, like multiplicity and transverse energy, provide very valuable information. Besides defining the collision geometry, they can be related to the initial energy density, e.g. using the well-known Bjorken relation [2], shed light into the mechanisms of particle production[3] and provide constraints to the many models aiming at describing these collisions [4].

The charged particle rapidity density at mid-rapidity has been measured by the four RHIC experiments -BRAHMS, PHENIX, PHOBOS and STAR- with very good agreement among their results [5]. For central Au-Au collisions at  $\sqrt{s_{NN}} = 130 \text{ GeV}$ , the global average is  $dN_{ch}/d\eta = 580 \pm 18$ . For the transverse energy rapidity density there is only one measurement, by PHENIX, with a value  $dE_T/d\eta = 578_{-39}^{+26} \text{ GeV}$  for the most central 2% of the inelastic cross section [6]. Using the Bjorken formula [2] this translates into an

initial energy density of  $\epsilon = 5.0 \text{ GeV}/fm^3$ <sup>2</sup> i.e. 60-70% larger than the corresponding values at the full SPS energy.

The energy dependence of the charged particle density  $dN_{ch}/d\eta$ , normalized to the number of participating nucleon pairs ( $N_{part}/2$ ), exhibits an almost logarithmic rise with  $\sqrt{s_{NN}}$  from AGS up to RHIC energies, as shown in Fig. 1. However, the dependence is very different from the  $p\bar{p}$  systematics also shown in Fig. 1. At  $\sqrt{s_{NN}} = 200 \text{ GeV}$ ,  $\sim 65\%$  more particles per pair of participants are produced in central Au-Au collisions than in  $p\bar{p}$ . Note also that the large increase predicted by the HIJING model with jet quenching [3] (upper curve in Fig. 1) is not observed, and from  $\sqrt{s_{NN}} = 130$  to  $200 \text{ GeV}$  the particle density increases by only 15% [5]. (See also Sections 2.2 and 6 for further discussion on jet quenching).

The centrality dependence of the charged particle density has been proposed as a sensitive tool to shed light on the particle production mechanism: soft processes are believed to scale with the number of participants  $N_{part}$ , whereas hard processes, expected to become more significant as the energy increases, lead to a scaling with the number of binary collisions  $N_{bin}$ . PHENIX [8] and PHOBOS [9] have reported an increase of  $dN_{ch}/d\eta$  and  $dE_T/d\eta$  strongly than linear with  $N_{part}$  (the PHENIX results are shown in Fig. 2 left panel) and in the framework of models with these two components, like HIJING [7, 11], such an increase is interpreted as evidence of the contribution of hard processes to particle production<sup>3</sup>. This is to be contrasted to SPS results where WA98 reports a much weaker increase (also shown in Fig. 2) [13] and WA97 an even weaker increase consistent within errors with proportionality with  $N_{part}$  [14]. Both the PHENIX and WA98 data, extrapolated to peripheral collisions, are in very good agreement with the  $p\bar{p}$  result at the same  $\sqrt{s}$  derived from the UA5 data [15]. The increased role of hard processes at higher energies and their scaling with  $N_{bin}$  could then explain the stronger increase of particle production in  $AA$  collisions compared to  $p\bar{p}$  previously discussed in the context of Fig. 1. The importance of hard processes at RHIC energies is a very interesting issue which will be further discussed in this review.

More surprising is the behavior of the ratio  $(dE_T/d\eta) / (dN_{ch}/d\eta)$ , the average transverse energy per charged particle, shown in Fig. 2 (right panel). This ratio is found to be independent of centrality and approximately equal to  $\sim 0.8 \text{ GeV}$ . Within errors of the order of 10-20% this ratio is also independent of  $\sqrt{s_{NN}}$  from AGS up to RHIC, implying a constant or a very moderate increase of the average  $p_T$  per particle.

It is also interesting to note that UA1 quotes a very similar ratio at  $\sqrt{s} = 200 \text{ GeV}$  [16] but with a rather large error of  $\sim 20\%$ . This seemingly universal behaviour of constant energy/particle is one of the most puzzling results. The increase in  $dE_T/d\eta$  with  $\sqrt{s_{NN}}$  translates into an increase in the number of produced particles rather than in the production of particles with larger  $E_T$ .

<sup>2</sup>using the canonical formation time  $\tau = 1 \text{ fm}/c$ . Much shorter formation times, as advocated in saturation models [7], would result in energy densities as high as  $\epsilon \simeq 20 \text{ GeV}/fm^3$ .

<sup>3</sup>This is, however, not a unique interpretation. The centrality dependence results of PHENIX shown in Fig. 2 have also been explained with a model based on purely soft processes [12].

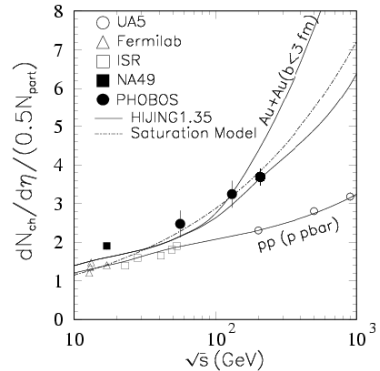


Figure 1: Energy dependence of charged particle density in central  $AA$  and  $pp$  collisions [3].

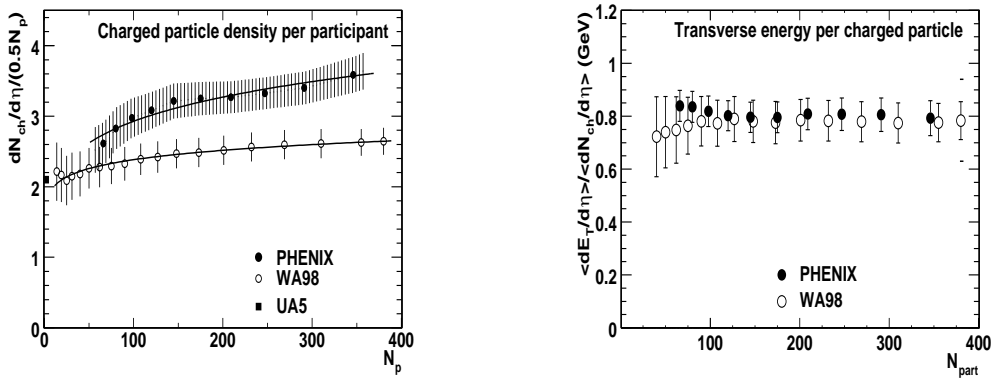


Figure 2: Left panel: Centrality dependence of the charged particle density from PHENIX and WA98 [10]. Right panel: Average  $E_T$  per charged particle from PHENIX and WA98 [6].

## 2.2 Elliptic flow

Elliptic flow originates from the spatial anisotropy of the diamond shaped system formed in non-central collisions, later converted into momentum anisotropy if enough rescatterings among particles occur in the further evolution of the system. Elliptic flow provides therefore an opportunity to learn about the degree of thermal equilibrium achieved with emphasis on the early collision dynamics.

Elliptic flow has been measured at RHIC by STAR [17], PHOBOS [18] and PHENIX [19] using different analysis methods and with good agreement between their results. The magnitude of elliptic flow, quantified e.g. by the second Fourier coefficient  $v_2$  of the azimuthal particle distribution with respect to the reaction plane, is shown in Fig. 3 (left panel) as function of beam energy. The strength of  $v_2$  at RHIC follows the systematic trend established over a very broad range of lower energies from SIS to SPS. The STAR value of 6% is approximately 50% larger than at the SPS, suggesting a much stronger early approach to local thermal equilibrium at RHIC.

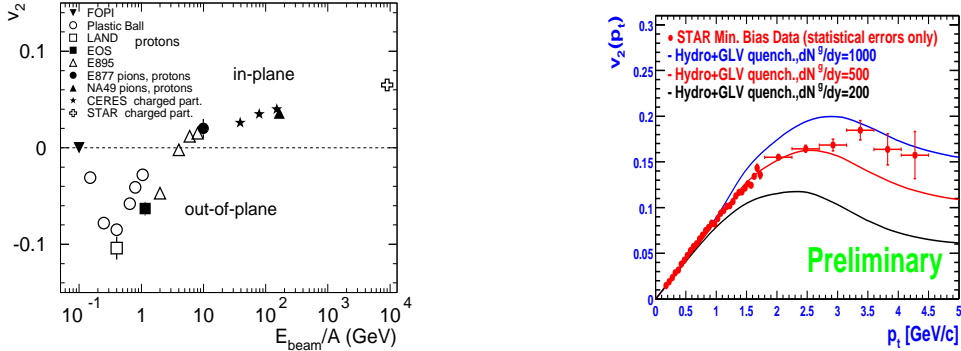


Figure 3: Left panel: Elliptic flow vs beam energy [20]. Right panel: Elliptic flow vs  $p_T$  measured by STAR in Au-Au collisions at  $\sqrt{s_{NN}} = 130 \text{ GeV}$  [21]. Curves represent hydrodynamic calculations with parton energy loss assuming different gluon densities  $dN^g/dy$  [22].

Other interesting features appear in the  $p_T$  dependence of  $v_2$  shown in Fig. 3 (right panel) [21]. Up to  $p_T$  of  $1 \text{ GeV}/c$ , hydrodynamic calculations, which implicitly assume local thermal equilibrium, are in remarkably good agreement with the data, contrary

to the observations at the SPS where the experimental results are significantly below the hydrodynamic limit [23]. At higher  $p_T$ , when pQCD starts to become significant,  $v_2$  appears to saturate. This behaviour can be reproduced by incorporating in the hydrodynamic model the energy loss of hard partons (jet quenching) in a dense medium with an initial gluon density of  $dN^g/dy \sim 500 - 1000$  [22]<sup>4</sup>. This novel feature of jet quenching is further discussed in Section 6.

## 2.3 Particle interferometry

Two-particle correlation with small relative momentum (HBT) is a useful tool to learn about the lifetime and size of the source at the time of particle emission. Since pions and kaons are emitted rather late, these correlations provide information about the space-time extent of the hadron system in the later stages of the collision. The HBT technique

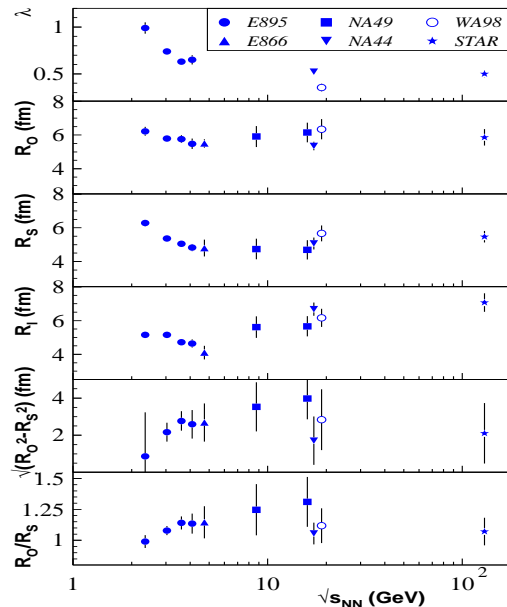


Figure 4: Energy dependence of  $\pi^-$  HBT parameters [26].

has been widely used in ion experiments over the past decade at the AGS and SPS [25] and first results from RHIC on pion interferometry are already available [26, 27]. The systematic behaviour of the source parameters –the radii  $R_o$ ,  $R_s$ ,  $R_l$  and the coherence parameter  $\lambda$ –, as function of energy is displayed in Fig.4. The RHIC results are a big puzzle. All HBT parameters have almost the same values as at the SPS. In particular, the larger source size  $R_s$  and longer source lifetime reflecting itself in  $R_o/R_s \geq 2$ , expected if a QGP is formed [28], are not observed at RHIC. Instead,  $R_s$  is very close to the SPS value and  $R_o/R_s \sim 1$  again as at the SPS. These results are surprising and raise questions about the present understanding of the space-time evolution of relativistic heavy-ion collisions.

<sup>4</sup>This might not be a unique interpretation. In a very recent paper, the  $v_2$  saturation at high  $p_T$  is explained by the two-particle correlation of produced minijets [24].

### 3 HADRONIC OBSERVABLES

Hadronic observables (spectra of identified particles, ratios of particle/antiparticle production, absolute particle yields) contribute, together with the global observables discussed in the previous section, to complete our view of the space-time evolution of RHI collisions. From their systematic studies, the picture has emerged of an initial high density state, which quickly reaches equilibrium and cools down while undergoing collective expansion. Particles decouple when the temperature and thus the particle density are low enough that interactions stop. We distinguish the chemical freeze-out when inelastic collisions cease to occur and particle abundances are frozen and the kinetic freeze-out, occurring later and at a lower temperature, when elastic processes stop and transverse momenta are frozen.

#### 3.1 Chemical freeze-out

If we assume that an ideal hadron gas in thermal equilibrium is formed, then, in a statistical model using the grand canonical ensemble, the final particle production ratios are governed by only two independent variables, the temperature  $T$  and the baryochemical potential  $\mu_B$  characterizing the system at chemical freeze-out [29]. This simple model works extremely well and reproduces all data available from SIS, AGS, SPS and also the new data from RHIC. It is interesting to note that the enhanced production of strange and multi-strange hadrons, one of the first proposed signatures of QGP formation, is also described by the statistical model nearly as well as all other species.

The parameters  $T$  and  $\mu_B$  derived from SPS and RHIC data are listed in Table 1 [29, 30].

Table 1: Chemical freeze-out parameters (temperature  $T$  and baryochemical potential  $\mu_B$ ) derived from SPS [29] and RHIC data [30]

	SPS	RHIC
$T$ (MeV)	$168 \pm 5$	$175 \pm 7$
$\mu_B$ (MeV)	$\sim 270$	$51 \pm 6$

The temperatures are practically the same at RHIC and SPS, whereas  $\mu_B$  is considerably lower at RHIC reflecting a lower net baryon density (see below). However, at both SPS and RHIC, the freeze-out parameters in the  $T$  vs  $\mu_B$  plane are close to the expected boundaries of the QGP phase transition. So presumably, prior to freeze-out, the system was in a deconfined or at least in a mixed phase.

#### 3.2 Kinetic freeze-out

The conditions at kinetic freeze-out are derived from the transverse momentum spectra of identified particles. As an example, Fig. 5 shows the positive and negative  $p$ ,  $K$ ,  $\pi$  spectra measured by PHENIX in central Au-Au collisions at  $\sqrt{s_{NN}} = 130$  GeV [31]. The spectra exhibit an almost exponential shape with a temperature  $T$  (the inverse slope parameter) increasing with particle mass. This qualitative behaviour is independent of  $\sqrt{s_{NN}}$ . It has been observed all the way from BEVALAC up to RHIC energies and can be understood if one postulates that there is collective radial flow on top of the thermal chaotic contribution [32], so that that the measured inverse slope  $T = T_{fo} + m \langle \beta_T \rangle^2$ .

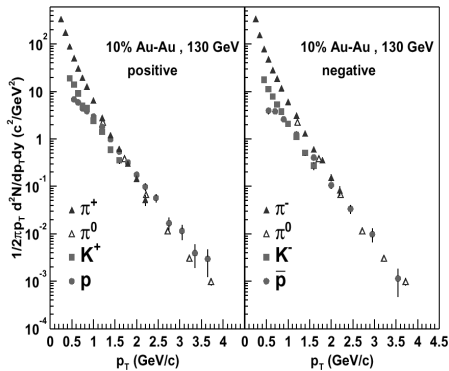


Figure 5: Identified particle spectra measured by PHENIX in central Au-Au collisions at  $\sqrt{s_{NN}} = 130 \text{ GeV}$  [31].

Particle spectra are then reproduced with only two parameters, characterizing the system at kinetic freeze-out, the freeze-out temperature  $T_{fo}$  and the collective radial flow velocity  $\langle \beta_T \rangle$ .  $T_{fo}$  is basically constant at  $\sim 130 \text{ MeV}$  from AGS to RHIC as expected if particles decouple at a given density. A constant radial flow velocity of  $\langle \beta_T \rangle \sim 0.4$  has been established at AGS and SPS energies, whereas the first RHIC results point to a higher value of  $\sim 0.6$  indicating higher initial pressure in the system. The resulting larger inverse slopes lead to an interesting feature not observed at lower energies. The  $\bar{p}$  and  $\pi^-$  (as well as the  $p$  and  $\pi^+$ ) yields become comparable at  $p_T \approx 2 \text{ GeV}/c$ .

At the SPS, the  $\Omega$  and  $J/\psi$  (and probably also the  $\Xi$ ) particles follow a different pattern [37]. They exhibit stronger slopes than expected from the previously quoted formula. This is taken as evidence that these particles decouple earlier from the system due to their relatively large mean free path. It will be very interesting to see whether similar data from RHIC will follow the same pattern.

### 3.3 Baryon yields

Baryon yields have consistently attracted interest: (i) the net baryon yield at mid-rapidity is an important observable allowing to study the amount of baryon stopping (the transport of participating nucleons to mid-rapidity) that occurs early in the collision. (ii) the mechanism of baryon stopping is an unsolved question and a topic of recent debate [33, 34]. (iii) the total baryon density plays an important role in connection with in-medium modification of light vector mesons and low-mass dilepton production as emphasized recently [35] (see Section 4).

The  $\bar{p}/p$  and  $\bar{\Lambda}/\Lambda$  ratios increase dramatically from values of  $\sim 0.1$  at SPS to values of  $\sim 0.7$  at RHIC [31, 36, 37, 38]. Clearly the ratios do not yet reach unity. The system approaches net baryon free conditions, but remarkably, still  $\sim 5\%$  of the participating nucleons are transported over 5 units of rapidity as shown in Table 2.

From the inclusive (i.e. non-corrected for feed-down) measurement of  $p$  and  $\bar{p}$  one can get a crude estimate of the total baryon density (under the assumption that  $p$  and  $n$  have the same stopping probability, that  $p\bar{p}$  and  $n\bar{n}$  pairs are produced in equal quantities and that higher mass baryons (mainly lambdas and sigmas) finally end up as  $p, \bar{p}, n$  or  $\bar{n}$ ). The relevant quantities for RHIC are listed in Table 2. A similar estimate at the maximum SPS energy of  $\sqrt{s_{NN}} = 17 \text{ GeV}$ , derived from the feed-down corrected  $p, \bar{p}$  yields and the  $\Lambda, \bar{\Lambda}$  yields [39] gives a total baryon density of  $dN_B/dy = 110$ . It appears therefore that, contrary to previous expectations, the total baryon density is approximately the same at

Table 2: Net and total baryon density at RHIC

RHIC Au-Au at $\sqrt{s_{NN}} = 130 GeV$	
$dN(p)/dy$	28.7 <sup>a</sup>
$dN(\bar{p})/dy$	21.1 <sup>a</sup>
Net protons $dN(p - \bar{p})/dy$	8.6
Participating Nucleons $(p - \bar{p})A/Z$	21.4
Produced Baryons $(p, \bar{p}, n, \bar{n})$	80.4
Total Baryon Density $dN_B/dy$	102

a) inclusive  $p$  and  $\bar{p}$  rapidity density from [31]

SPS and RHIC, the strong decrease in nuclear stopping being compensated by copious production of baryon-antibaryon pairs.

## 4 LOW-MASS $e^+e^-$ PAIRS and PHOTONS

Dileptons and photons are unique probes to study the dynamics of relativistic heavy-ion collisions [40]. The interest stems from their relatively large mean free path. As a consequence, they can leave the interaction region without final state interaction, carrying information about the conditions and properties of the matter at the time of their production and in particular at the early stages when deconfinement and chiral symmetry restoration have the best chances to occur.

The prominent topic of interest, both in dileptons and photons, is the identification of thermal radiation emitted from the collision system. This radiation should tell us the nature of the matter formed, a quark-gluon plasma (QGP) or a high-density hadron gas (HG). The physics potential of low-mass dileptons is further augmented by their sensitivity to chiral symmetry restoration. The  $\rho$ -meson is the prime agent here. Due to its very short lifetime ( $\tau = 1.3 fm/c$ ) compared to the typical fireball lifetime of  $\sim 10 fm/c$  at SPS energies, most of the  $\rho$  mesons decay inside the interaction region providing a unique opportunity to observe in-medium modifications of particle properties (mass and/or width) which might be linked to chiral symmetry restoration. The situation is different for the  $\omega$  and  $\phi$  mesons. Because of their much longer lifetimes they predominantly decay outside the interaction region after having regained their vacuum properties. The  $\omega$  and  $\phi$  mesons remain nevertheless important messengers: the undisturbed  $\omega$  can serve as a reference and the  $\phi$  with its  $s\bar{s}$  content is a probe of strangeness production.

For the moment, the stage for low-mass dileptons belongs to CERN and more specifically to the CERES experiment. CERES has systematically studied the production of  $e^+e^-$  pairs in the mass region  $m \leq 1.0 GeV/c^2$ , with measurements of p-Be, p-Au, [41, 42], S-Au [43] and Pb-Au [45, 46, 20]. Whereas the  $p$  data are well reproduced by the known hadronic sources, a strong enhancement is observed in the mass region  $200 < m < 600 MeV/c^2$  both in the S and Pb data with respect to those sources scaled to the nuclear case with the event multiplicity. Fig. 6 (left panel) shows the results from Pb-Au collisions at  $40 A GeV$  with an enhancement factor of  $5.1 \pm 1.3(stat.)$  relative to the hadronic cocktail. Within uncertainties, this is consistent with, or even larger than, the enhancement factor of  $2.9 \pm 0.3(stat.) \pm 0.6(syst.)$  obtained from the combined



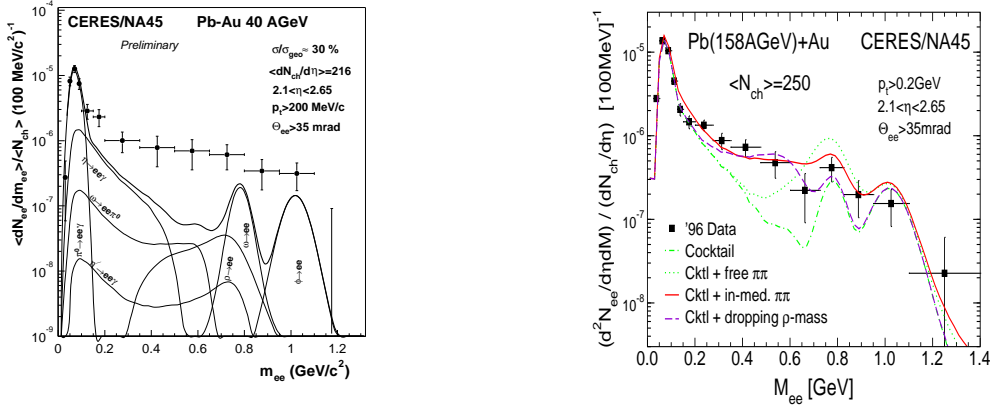


Figure 6: Left panel: Invariant mass  $e^+e^-$  spectrum measured by CERES in 40  $A$   $GeV$  Pb-Au collisions [20]. The figure also shows the summed (thick solid line) and individual contributions from hadronic sources. Right panel: Comparison of CERES 96 results from Pb-Au collisions at 158  $A$   $GeV$  with various theoretical approaches (see text).

95-96 Pb-Au data at 158  $A$   $GeV$ . Further studies on the latter demonstrate that the enhancement is more pronounced at low pair  $p_T$  and increases faster than linearly with the event multiplicity. In all cases, with the S and Pb beam, the enhancement sets at  $m \geq 2m_\pi$ .

The enhancement of low-mass dileptons has triggered a wealth of theoretical activity (for a comprehensive review see [47]). There is consensus that a simple superposition of  $pp$  collisions cannot explain the data and that an additional source is needed. The pion annihilation channel ( $\pi^+\pi^- \rightarrow \rho \rightarrow l^+l^-$ ), obviously irrelevant in  $pp$  collisions, has to be added in the nuclear case. This channel accounts for a large fraction of the observed enhancement (see line cocktail + free  $\pi\pi$  in Fig. 6 right panel) and provides first evidence of thermal radiation from a dense hadron gas. However, in order to quantitatively reproduce the data in the mass region  $0.2 < m_{e^+e^-} < 0.6 \text{ GeV}/c^2$ , it was found necessary to include in-medium modifications of the  $\rho$  meson. Li, Ko and Brown [48], following the original Brown-Rho scaling [49], proposed a decrease of the  $\rho$ -mass in the high baryon density of the fireball, as a precursor of chiral symmetry restoration, and achieved excellent agreement with the CERES data (see the line cocktail + dropping mass in Fig. 6 right panel).

Another avenue, based on effective Lagrangians, uses the broadening of the  $\rho$ -meson spectral function resulting from its propagation in the medium, mainly from scattering off baryons [50], and achieves also an excellent reproduction of the CERES data (see line cocktail + in-medium  $\pi\pi$  in Fig. 6 right panel). The success of these two different approaches, one relying on quark degrees of freedom and the other on a pure hadronic model, has attracted much interest. Rapp raised, and provided support for, the hypothesis of quark-hadron duality down to low-masses by showing that in a high density state the dilepton production rates calculated with the in-medium  $\rho$ -meson spectral function are very similar to the  $q\bar{q}$  annihilation rates calculated in pQCD [51]. It is interesting to note that the 40  $A$   $GeV$  data is also equally well reproduced by the two approaches [20]. The accuracy of the data does not allow to discriminate among the two. The CERES run of year 2000 taken with improved mass resolution and good statistics may allow to do that.

The extension of these studies to RHIC energies should be very interesting. The total baryon density, which is the key factor responsible for in-medium modifications

of the  $\rho$  meson both in the dropping mass and the collision broadening scenarios, is almost as high at RHIC as at SPS (cf. Section 3.3), contrary to previous expectations. Updated RHIC predictions that incorporate this and other acquired knowledge on global and hadronic observables, show indeed that the enhancement of low-mass  $e^+e^-$  pairs persist at the collider with at least comparable strength [52]. The calculations further predict in-medium modifications of the  $\omega$  and  $\phi$  mesons. These are much less dramatic than in the case of the  $\rho$  meson but should nevertheless be readily observable with the excellent mass resolution of the PHENIX detector. First results on single electrons from PHENIX are already available [53] and results on the  $\phi$  meson from the second RHIC run are expected soon. The combined analysis of  $\phi \rightarrow K^+K^-$  and  $\phi \rightarrow e^+e^-$  within the same apparatus should provide a very powerful diagnostic tool to make evident in-medium effects.

Direct photons are expected to provide analogous information to thermal dileptons. However, the physics background for real photons is larger by orders of magnitude compared to dileptons making the measurement of photons much tougher and less sensitive to a new source. And indeed, only a small direct photon signal of  $\sim 20\%$  has been observed in central Pb-Au collisions by the WA98 experiment [54]. The better conditions at RHIC, larger particle densities and hence larger initial temperatures should provide a more compelling evidence of this key signal.

## 5 $J/\psi$ SUPPRESSION

The melting of charmonium states in a deconfined state of matter is one of the earliest signatures of QGP formation [55] and has provided one of the most exciting sagas of the SPS programme. Already in the first runs with O and S beams, the NA38/NA50 experiment observed a suppression of  $J/\psi$  which immediately captured the interest. Intensive theoretical efforts were devoted to explain the effect within conventional physics and it soon appeared that all experimental data, including systematic studies of  $pp$ ,  $pA$  and  $SU$  collisions, can be reproduced by invoking the absorption in nuclear medium of the  $c\bar{c}$  pair before it forms a  $J/\psi$ , with a cross section  $\sigma_{abs} = 6.4 \pm 0.8 mb$  [56].

However, a different behavior is observed with the 158 A GeV Pb beam. Whereas peripheral collisions seem to follow the regular absorption pattern, an anomalously larger suppression occurs at central collisions characterized by impact parameters  $b < 8 fm$  or  $E_T > 40 GeV$  which can be translated into a Bjorken energy density  $\epsilon > 2.3 GeV/fm^3$  (see Fig. 7) [57]. The data in this figure exhibit a two-step suppression pattern which NA50 attributes to the successive melting of the  $\chi_c$  and directly produced  $J/\psi$  mesons in a quark-gluon plasma scenario.

The same data normalized to the Drell-Yan cross section are shown in Fig. 8 as function of  $E_T$ . The two-step pattern can be discerned here at  $E_T$  values of  $\sim 30$  and  $\sim 100 GeV$ . Most published calculations, based on conventional hadronic models including the effect of absorption by comovers, fail to reproduce the

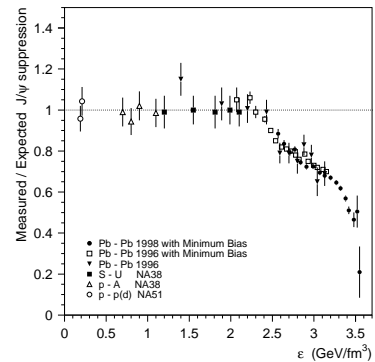


Figure 7: Measured over expected (assuming normal absorption cross section)  $J/\psi$  yield vs. energy density [57].

results as illustrated in the left panel of Fig. 8. The recent calculations of Capella et al. [58] are in much better agreement with the data and fail only at the most central collisions (middle panel). On the other hand, quite good agreement over the whole  $E_T$

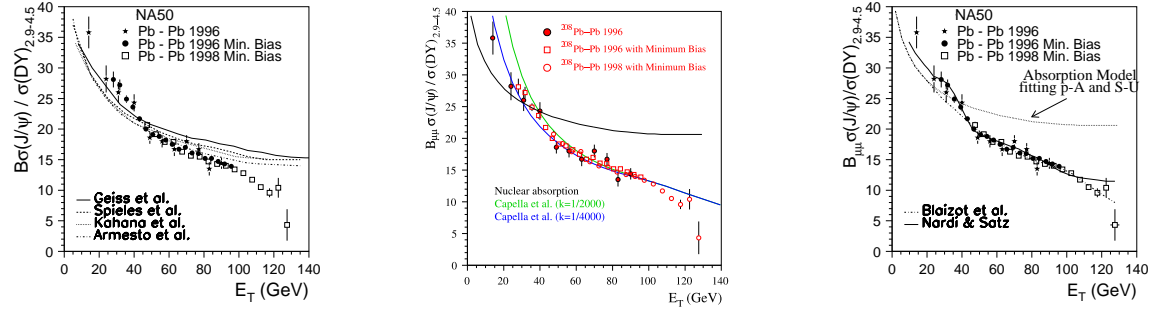


Figure 8:  $J/\psi$  over Drell-Yan cross section vs.  $E_T$  measured by NA50 in Pb-Pb collisions at  $\sqrt{s_{NN}} = 17.2 \text{ GeV}$  in comparison to various theoretical approaches using conventional physics (left and middle panels) and quark matter formation (right panel) (taken from [62]).

range is achieved by models assuming QGP formation (right panel) [59, 61]. The model of Blaizot et al. reproduce the data remarkably well by invoking  $J/\psi$  suppression whenever the energy density exceeds the critical value for deconfinement (first step) together with fluctuations of the transverse energy for the most central collisions (second step) [59].

The extrapolation of these results to RHIC energies is not at all clear and ranges from total suppression up to enhancement ! [60] thus ensuring another exciting chapter on the  $J/\psi$  saga. First glimpse on  $J/\psi$  production at RHIC is expected from the PHENIX results of year 2 run.

## 6 SUPPRESSION OF LARGE $p_T$ HADRONS

With the energies available at RHIC, one order of magnitude higher than at the SPS, new channels and probes become accessible for matter diagnostics. In particular, energy loss through gluon radiation of high  $p_T$  partons resulting from initial hard scattering and jet production has been predicted as a possible signature of deconfined matter. The phenomenon, commonly referred to as jet quenching, has been extensively studied over the last decade [63] and should manifest itself as a suppression of high  $p_T$  particles. Such a suppression has been observed already in the first low-luminosity RHIC run by the two large experiments STAR [21] and PHENIX [64] and certainly constitutes the most interesting result from RHIC so far. The suppression is evidenced by plotting the so-called nuclear modification factor [65] defined as the ratio of  $AA$  to  $pp$   $p_T$  spectra, scaled by the number of binary collisions:

$$R_{AA}(p_T) = \frac{d^2\sigma_{AA}/dp_T d\eta}{\langle N_{bin} \rangle d^2\sigma_{pp}/dp_T d\eta}$$

In the absence of any new physics this ratio should be equal to 1 at the high  $p_T$  characteristic of hard processes. At low  $p_T$ , dominated by soft processes which scale with the number of participants, the ratio is expected to be lower, e.g. for central

collisions  $R_{AA}(0) \approx 0.5N_{part}/N_{bin} \approx 0.2$ . The STAR and PHENIX results for central Au-Au collisions at  $\sqrt{s_{NN}} = 130 \text{ GeV}$  are shown in Fig. 9. In both cases the  $pp$  data at  $130 \text{ GeV}$  were derived from interpolation of  $pp$  data [16, 66, 67] at lower and higher energies. STAR shows the ratio for negative hadrons and PHENIX for negative hadrons

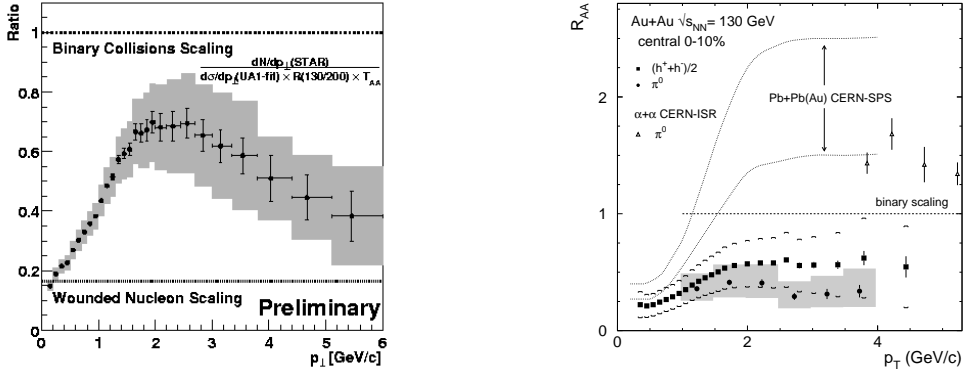


Figure 9: High  $p_T$  suppression in Au-Au collisions at  $\sqrt{s_{NN}} = 130 \text{ GeV}$  measured by STAR for negative hadrons (left panel) [21] and in PHENIX for negative hadrons and  $\pi^0$  (right panel) [64].

as well as identified  $\pi^0$ . As expected, for low  $p_T$  the ratio is small,  $\approx 0.2$ . It raises with  $p_T$ , getting close to unity and then falls off at higher  $p_T$  in the STAR data whereas it seems to flatten in the PHENIX data. The suppression appears to be stronger for  $\pi^0$  than for charged particles. This implies that the ratio  $\pi^0/h$  is considerably smaller than unity and reflects the large  $p, \bar{p}$  contribution to the charged particle spectra at high momentum (cf. Section 3.2). A similar suppression pattern appears when the ratio of central to peripheral collisions, each divided by its corresponding value of  $N_{bin}$ , is plotted as function of  $p_T$  [64]. This behaviour is in marked contrast to the observations in Pb-Pb and Pb-Au collisions at the SPS (the solid lines in Fig. 9 right panel represent the band of uncertainty of the CERN results) where the ratio overshoots unity and saturates at high  $p_T$ , like in pA collisions [65] due to the well known Cronin effect [68]. The high  $p_T$  suppression observed at RHIC can be quantitatively reproduced in terms of jet quenching if an average energy loss of  $dE/dx \approx 0.25 \text{ GeV}/fm$  is assumed within a parton model[69].

In the context of the new RHIC data, jet quenching has been discussed in three different topics (cf. Sections 2.1, 2.2 and this Section). Whereas the phenomenon helps describing the observed effects in elliptic flow and high  $p_T$  suppression, the expected increase in particle production has not been observed (cf. Section 2.1). Fine tuning of the theoretical treatment to achieve consistent description of all these observables together with new RHIC data allowing to reach much higher  $p_T$  values and reference data on  $pp$  and  $pA$  measured within the same apparatus will be very valuable to consolidate these intriguing results.

## 7 CONCLUSION

In a relatively short run, the RHIC experiments have produced an impressive amount of results and much more is expected over the next years. The second RHIC run has just been completed with a recorded luminosity almost two orders of magnitude larger than

in year-1. This, together with the still ongoing yield of interesting results from the SPS programme, places the field of relativistic heavy-ion collisions at a very unique phase with exciting physics prospects.

## References

- [1] Proceedings of Quark Matter 2001 in Nucl. Phys. **A698**, (2002).
- [2] J.D. Bjorken, Phys. Rev. **D27**, 140 (1983).
- [3] X.N. Wang and M. Gyulassy, Phys. Rev. Lett. **86**, 3496 (2001).
- [4] S.A. Bass et al, Nucl. Phys. **A661**, 205c (1999).
- [5] B.B. Back et al., PHOBOS Coll., Phys. Rev. Lett. **88**, 022302 (2002).
- [6] K. Adcox et al., PHENIX Coll., Phys. Rev. Lett. **87**, 052301 (2001).
- [7] D. Kharzeev and M. Nardi, Phys. Lett. **B507**, 121 (2001).
- [8] K. Adcox et al., PHENIX Coll., Phys. Rev. Lett. **86**, 3500 (2001).
- [9] B.B. Back et al., PHOBOS Coll., Preprint nucl-ex/0201005.
- [10] A. Milov for the PHENIX Collaboration, Nucl. Phys. **A698**, 171c (2002).
- [11] X.N. Wang and M. Gyulassy, Phys. Rev. **D44**, 3501 (1991).
- [12] A. Capella and D. Sousa, Phys. Lett. **B511**, 185 (2001).
- [13] M.M. Aggarwal et al., WA98 Coll., Eur. Phys. J, **C18**, 651 (2001).
- [14] F. Antinori et al, WA97 Coll., Eur. Phys. J. **C18**, 57 (2000).
- [15] G.J. Alner et al., UA5 Coll., Z. Phys. **C33**, 1 (1986).
- [16] C. Albajar, UA1 Coll., Nucl. Phys. **B335**, 261 (1990).
- [17] K.H. Ackermann, STAR Coll., Phys. Rev. Lett. **86**, 402 (2001).
- [18] I. Park, PHOBOS Coll., Nucl. Phys. **A698**, 564c (2002).
- [19] W.A. Zajc for the PHENIX Coll., Nucl. Phys. **A698**, 39c (2002) and K. Adcox et al., PHENIX Coll., to be submitted to Phys. Rev. Lett.
- [20] H. Appelshauser for the CERES Coll., Nucl. Phys. **A698**, 253c (2002).
- [21] J. Harris for the STAR Coll., Nucl. Phys. **A698**, 64c (2002).
- [22] M. Gyulassy, I. Vitev and X.N. Wang, Phys. Rev. Lett. **86**, 2537 (2001).
- [23] P.F. Kolb, P. Huovinen, U. Heinz and H. Heiselberg, Phys. Lett. **B500**, 232 (2001).
- [24] Y.V. Kovchegov and K. Tuchin, Preprint hep-ph/0203213.

- [25] U.A. Wiedemann and U. Heinz, Phys. Rep. **319**, 145 (1999).
- [26] C. Adler et. al., STAR Coll., Phys. Rev. Lett. **87**, 082301 (2001).
- [27] K. Adcox et al., PHENIX Coll., Phys. Rev. Lett. in press, nucl-ex/0201008.
- [28] D.H. Rischke and M. Gyulassy, Nucl. Phys. **A608**, 479 (1996).
- [29] P. Braun-Munzinger, I. Heppe and J. Stachel, Phys. Lett. **B465**, 15 (1999).
- [30] P. Braun-Munzinger, D. Magestro, K. Redlich and J. Stachel, Phys. Lett. **B518**, 41 (2001).
- [31] K. Adcox et al., PHENIX Coll., Phys. Rev. Lett. in press, nucl-ex/0112006.
- [32] E. Schnedermann et al., Phys. Rev. **C48**, 2462 (1993).
- [33] D. Kharzeev, Phys. Lett. **B378**, 238 (1996).
- [34] S. Vance, M. Gyulassy and X.N. Wang, Phys. Lett. **B443**, 45 (1998).
- [35] R. Rapp, Phys. Rev. **C63**, 54907 (2001).
- [36] C. Adler et al., STAR Coll., nucl-ex/0203016.
- [37] N. Xu and M. Kaneta Nucl. Phys. **A698**, 306c (2002).
- [38] K. Adcox et al., PHENIX Coll., (in preparation).
- [39] J. Bachler et al., NA49 Coll., Nucl. Phys. **A661**, 45c (1999), S.M. Afanasiev, NA49 Coll., nucl-ex/0201012, and T.Susa for the NA49 Coll., Nucl. Phys. **A698**, 491c (2002).
- [40] E.V. Shuryak, Phys. Lett. **B78**, 150 (1978).
- [41] G. Agakichiev et al., CERES Coll., Eur. Phys. J. **C4**, 231 (1998).
- [42] G. Agakichiev et al., CERES Coll., Eur. Phys. J. **C4**, 249 (1998).
- [43] G. Agakichiev et al., CERES Coll., Phys. Rev. Lett. **75**, 1272 (1995).
- [44] I. Ravinovich, for the CERES Coll., Nucl. Phys. **A638**, 159c (1998).
- [45] G. Agakichiev et al., CERES Coll., Phys. Lett. **B422**, 405 (1998).
- [46] B. Lenkeit, for the CERES Coll., Nucl. Phys. **A661**, 23 (1999).
- [47] R. Rapp and J. Wambach, Adv. Nucl. Phys. **25**, 1 (2000).
- [48] G.Q. Li, C.M. Ko and G.E. Brown, Phys. Rev. Lett. **75**, 4007 (1995).
- [49] G.E. Brown and M. Rho, Phys. Rev. Lett. **66**, 2720 (1991) and Phys. Rep. **269**, 333 (1996).

- [50] R. Rapp, G. Chanfray and J. Wambach, Nucl. Phys. **A617**, 472 (1997). and J. Wambach, Nucl. Phys. **A638**, 171c (1998).
- [51] R. Rapp, Nucl. Phys. **A661**, 33 (1999).
- [52] R. Rapp, nucl-th/0204003.
- [53] K. Adcox et al., PHENIX Coll., Phys. Rev. Lett. in press, nucl-ex/0202002.
- [54] M.M. Aggarwal et al., WA98 Collaboration, Phys. Rev. Lett. **85**, 3595 (2000).
- [55] T. Matsui and H. Satz, Phys. Lett. **B178**, 416 (1986).
- [56] M.C. Abreu et al., NA38 Coll., Phys. Lett. **B449**, 128 (1999) and Phys. Lett. **B466**, 408 (1999).
- [57] M.C. Abreu et al., NA50 Coll., Phys. Lett. **B477**, 28 (2000).
- [58] A. Capella et al., Phys. Rev. Lett. **85**, 2080 (2000).
- [59] J.P. Blaizot et al., Phys. Rev. Lett. **85**, 4012 (2000).
- [60] R.L. Thews, M. Schroether and J. Rafelski, Phys. Rev. **C63**, 054905 (2001) and P. Braun-Munzinger and J. Stachel, Phys. Lett. **B490**, 196 (2000).
- [61] M. Nardi and H. Satz, Phys. Lett. **B442**, 14 (1998).
- [62] P. Bordalo for the NA50 Coll., Nucl. Phys. **A698**, 127c (2002).
- [63] X.N. Wang and M. Gyulassy Phys. Rev. **D44**, 3501 (1991) and Phys. Rev. Lett. **68**, 1480 (1992).
- [64] K. Adcox et al., PHENIX Coll., Phys. Rev. Lett. **88**, 022301 (2001).
- [65] E. Wang and X.N. Wang, Phys. Rev **C64**, 034901 (2001).
- [66] B. Alper et al., Nucl. Phys. **B100**, 237 (1975).
- [67] F. Abe et al., CDF Coll., Phys. Rev. Lett. **61**, 1819 (1988).
- [68] D. Antreasyan et al., Phys. Rev. **D19**, 764 (1979).
- [69] X.N. Wang, Nucl. Phys. **A698**, 296C (2002).